Proceeding Paper

Simulations of Sky Radiances in Red and Blue Channels at Various Aerosol Conditions Using Radiative Transfer Modeling [†]

Christos-Panagiotis Giannaklis [1,*], Stavros-Andreas Logothetis [1], Vasileios Salamalikis [2], Panayiotis Tzoumanikas [1], Konstantinos Katsidimas [1] and Andreas Kazantzidis [1]

[1] Laboratory of Atmospheric Physics, Department of Physics, University of Patras, GR 26500 Patras, Greece; logothetiw_s@upnet.gr (S.-A.L.); tzumanik@ceid.upatras.gr (P.T.); katsidim@physics.upatras.gr (K.K.); akaza@upatras.gr (A.K.)

[2] NILU—Norwegian Institute for Air Research, 2027 Kjeller, Norway; vsal@nilu.no

[*] Correspondence: xristos_gia@hotmail.gr

[†] Presented at the 16th International Conference on Meteorology, Climatology and Atmospheric Physics—COMECAP 2023, Athens, Greece, 25–29 September 2023.

Abstract: We conducted a theoretical analysis of the relationship between red-to-blue (RBR) color intensities and aerosol optical properties. RBR values are obtained by radiative transfer simulations of diffuse sky radiances. Changes in atmospheric aerosol concentration (parametrized by aerosol optical depth, AOD), particle's size distribution (parametrized by Ångström exponent, AE) and aerosols' scattering (parametrized by single scattering albedo—SSA) lead to variability in sky radiances and, thus, affect the RBR ratio. RBR is highly sensitive to AOD as high aerosol load in the atmosphere causes high RBR. AE seems to strongly affect the RBR, while SSA effect the RBR, but not to such a great extent.

Keywords: aerosols; aerosol optical depth; angstrom exponent; RBR; radiative transfer modelling

1. Introduction

The accurate knowledge of the angular distribution of the diffuse sky radiance is crucial for many applications, particularly in building design [1], in design and performance investigation of photovoltaic (PV) systems [2,3], solar collectors and other spectral selective energy devices [4].

Aerosols' impact on the radiative balance of the Earth–Atmosphere system is caused by direct scattering and absorption (attenuation) of incoming solar radiation (direct impact) and through aerosol–cloud interactions (indirect impact). These interactions depend significantly on the aerosol load and aerosol optical properties like the aerosol optical depth (AOD), the Ångström exponent (AE) or the single scattering albedo (SSA) [5].

The diffuse sky radiance or luminance is strongly affected by aerosol optical properties under clear sky conditions [6,7]. Olmo et al. [8] used sky radiance measurements to study mineral dust optical properties, while Deering and Eck [9] investigated the effect of AOD in bi-directional reflectance distributions of vegetation canopies. Inversion algorithm has been implemented by different authors [10], e.g., Ref. [11] measured sky radiance to retrieve aerosol optical properties. Later, Dubovik et al. [12] and Olmo et al. [8] included non-spherical particles approximation in the previous proposed inversion codes to derive other aerosol properties, namely, size distribution, SSA, phase function (PF) and asymmetry parameter (g) from radiance measurements. The variation in sky radiance has been analyzed under various atmospheric conditions using measurements with instruments, such as spectroradiometers [13,14]. These spectral radiance observations have been compared with the results from radiative transfer models (RTM) mostly under clear sky conditions.

However, the limited number of radiometric stations around the globe and the cost of the equipment make it essential to explore alternative techniques. Recently, all-sky imagers (ASI) have been proven very useful for atmospheric applications since they automatically take series of hemispheric sky images.

All-sky images are devices that combine a digital camera with a fisheye lens that takes pictures of the full hemispherical sky and are based on measurements of radiance at three different wavelengths, which correspond to the red, green and blue spectral range. Furthermore, the red, green and blue (RGB) color intensity has gradually become one of the most widely used characteristics. Therefore, they can be used to obtain the spectral radiance distribution of the sky [15,16] and cloud and aerosol optical properties as well [17–19]. Specifically, the red-to-blue ratio (RBR) has been implemented in cloud detection algorithms of whole sky imagers [20–23], cloud segmentation [24,25], cloud classification [26], retrieving cloud characteristics [23,27], solar irradiance prediction and forecasting [28,29] and constructing clear-sky libraries (CSL) [30]. Image RBR is shown to be affected by aerosol conditions under cloud free sky conditions [31]. Reference [32] proposed a method that estimates the aerosol amount using the blue-to-red ratio within a vertical pixel line and compares it with AOD and particulate matter (PM) measurements.

This study aims to investigate the relationship between the RBR and aerosol optical properties, namely, AOD, AE and SSA, using simulated values of the red and blue color channels using a radiative transfer model (libRadtran) [33,34].

2. Methodology

The libRadtran software package (Mayer, B., Emde, C., and Kylling, A., LMU Munich, Munich, Germany) is widely used for radiative transfer calculations [33]. It enables the user to compute radiances, irradiances and actinic fluxes in both the solar and the thermal spectrums. The libRadtran package includes numerous tools that may be used to calculate the radiation field for given atmospheric and surface conditions.

In the current work, the libRadtran version 2.0.1 [34] and the UVSPEC radiative transfer model are adopted. The UVSPEC model includes various methods to solve the radiative transfer equations. The discrete ordinate solver DISORT (Discrete-Ordinate-Method Radiative Transfer) [35], which considers the atmosphere a non-isothermal, vertically inhomogeneous but horizontally homogeneous medium, is selected. AOD at 500 nm and AE are the varying input parameters. Using the "output rgb" option in libRadtran, sky radiances are automatically converted to RGB values. For every simulation, the solar zenith angle (SZA) is $30°$, and the RBR is calculated at the zenith point of the image and a number of scattering angles.

3. Results

Figure 1 display the scatter plots between RBR and AOD_{500nm} (a), AE (b) and SSA (c) for four different sky scattering angles. Based on Figure 1a, it can be observed that the RBR exhibits a quadratic growth as AOD increases, revealing that the red and blue radiances are equal for high AOD values. The RBR values were also related to scattering angles, encompassing lower values for lower scattering angles, which is strongly related to the aerosol scattering processes around the circumsolar region. Regarding AE, the RBR values followed a decreasing trend for coarse aerosol particles (AE < 0.6). Nevertheless, for higher AE values, the trends switch to increasing when the aerosol size becomes smaller. Finally, the RBR values documented a marginal linear decrease with increases in the SSA for all scattering angles. It is apparent that the wavelength-dependent scattering of light, and thus the RBR, is strongly related to the aerosol burden and to the aerosol size distribution.
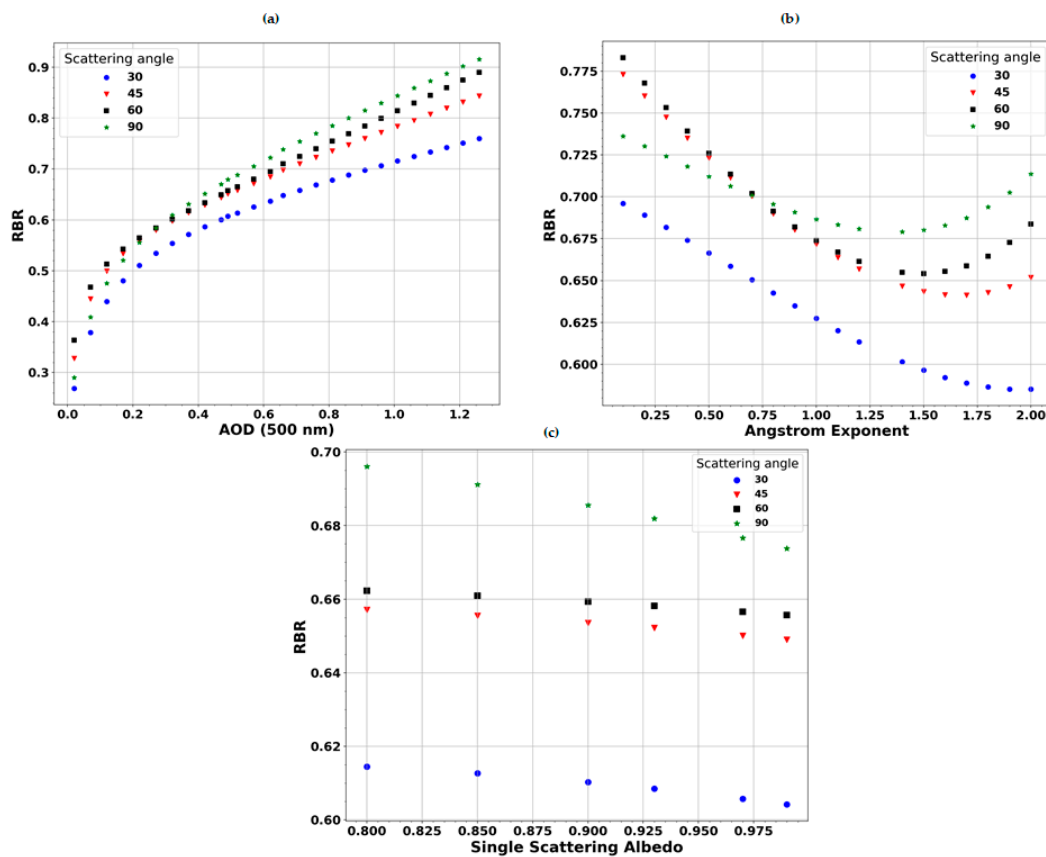
Figure 1. Scatter plots of RBR as a function of AOD at 500 nm (**a**), AE (**b**) and SSA (**c**) at various scattering angles (30°, 45°, 60°, 90°) from radiative transfer simulations.

4. Conclusions

Clear sky RBR varies significantly because of changes in atmospheric composition. The main objective of this study was to determine the impact of aerosol optical properties on RBR using radiative transfer modeling. High sensitivity between RBR and AOD was found; high aerosol burden in the atmosphere causes high RBR. As aerosol load increases, Mie scattering dominates over Rayleigh; thus, light is scattered equally along all wavelengths resulting in high RBR values even close to 0.9, when AOD at 500 nm reaches values higher than the unity, for large scattering angles. Aerosol particle size, parameterized by the AE, seems to strongly affect the ratio too, with high values of RBR detected for large particles (AE < 0.5). This is because most aerosols are of the same order of size or larger than the wavelength of incoming light. The single scattering albedo of the aerosols affects RBR, but not to such a great extent.

Institutional Review Board Statement: Not applicable.

Informed Consent Statement: Not applicable.

References

1. Li, D.H.; Lam, J.C. Evaluation of lighting performance in office buildings with daylighting controls. *Energy Build.* **2001**, *33*, 793–803. [CrossRef]
2. Plag, F.; Kröger, I.; Riechelmann, S.; Winter, S. Multidimensional model to correct PV device performance measurements taken under diffuse irradiation to reference conditions. *Sol. Energy* **2018**, *174*, 431–444. [CrossRef]
3. Behrendt, T.; Kuehnert, J.; Hammer, A.; Lorenz, E.; Betcke, J.; Heinemann, D. Solar spectral irradiance derived from satellite data: A tool to improve thin film PV performance estimations? *Sol. Energy* **2013**, *98*, 100–110. [CrossRef]
4. Li, D.H.; Lam, J.C. Predicting solar irradiance on inclined surfaces using sky radiance data. *Energy Convers. Manag.* **2004**, *45*, 1771–1783. [CrossRef]
5. Masson-Delmotte, V.; Zhai, P.; Pirani, A.; Connors, S.L.; Péan, C.; Berger, S.; Caud, N.; Chen, Y.; Goldfarb, L.; Gomis, M.I.; et al. *Climate Change 2021: The Physical Science Basis. Contribution of Working Group I to the Sixth Assessment Report of the Intergovernmental Panel on Climate Change*; Cambridge University Press: Cambridge, UK, 2021. [CrossRef]
6. Kreuter, A.; Emde, C.; Blumthaler, M. Measuring the influence of aerosols and albedo on sky polarization. *Atmos. Res.* **2010**, *98*, 363–367. [CrossRef] [PubMed]
7. Aiyan, G.; Jingshuang, C.; Aosong, Z.; Shanbao, H. Attenuation and sky radiance effects induced by atmospheric aerosols on satellite-ground optical communication links. In Proceedings of the 2017 IEEE 9th International Conference on Communication Software and Networks (ICCSN), Guangzhou, China, 6–8 May 2017; pp. 619–623. [CrossRef]
8. Olmo, F.; Quirantes, A.; Lara, V.; Lyamani, H.; Alados-Arboledas, L. Aerosol optical properties assessed by an inversion method using the solar principal plane for non-spherical particles. *J. Quant. Spectrosc. Radiat. Transf.* **2007**, *109*, 1504–1516. [CrossRef]
9. Deering, D.W.; Eck, T.F. Atmospheric optical depth effects on angular anisotropy of plant canopy reflectance. *Int. J. Remote Sens.* **1987**, *8*, 893–916. [CrossRef]
10. Tohsing, K.; Klomkliang, W.; Masiri, I.; Janjai, S. An investigation of sky radiance from the measurement at a tropical site. *AIP Conf. Proc.* **2017**, *1810*, 080006. [CrossRef]
11. Dubovik, O.; King, M.D. A flexible inversion algorithm for retrieval of aerosol optical properties from Sun and sky radiance measurements. *J. Geophys. Res. Atmos.* **2000**, *105*, 20673–20696. [CrossRef]
12. Dubovik, O.; Sinyuk, A.; Lapyonok, T.; Holben, B.N.; Mishchenko, M.; Yang, P.; Eck, T.F.; Volten, H.; Muñoz, O.; Veihelmann, B.; et al. Application of spheroid models to account for aerosol particle nonsphericity in remote sensing of desert dust. *J. Geophys. Res. Atmos.* **2006**, *111*, D11208. [CrossRef]
13. Ricchiazzi, P.J.; Payton, A. The Effect of Surface Albedo Heterogeneity on Sky Radiance. In Proceedings of the Tenth ARM Science Team Meeting Proceedings, San Antonio, TX, USA, 13–17 March 2000; pp. 1–9.
14. Kider, J.T.; Knowlton, D.; Newlin, J.; Li, Y.K.; Greenberg, D.P. A framework for the experimental comparison of solar and skydome illumination. *ACM Trans. Graph.* **2014**, *33*, 1–12. [CrossRef]
15. Rossini, E.G.; Krenzinger, A. Maps of sky relative radiance and luminance distributions acquired with a monochromatic CCD camera. *Sol. Energy* **2007**, *81*, 1323–1332. [CrossRef]
16. Román, R.; Antón, M.; Cazorla, A.; De Miguel, A.; Olmo, F.J.; Bilbao, J.; Alados-Arboledas, L. Calibration of an all-sky camera for obtaining sky radiance at three wavelengths. *Atmos. Meas. Tech.* **2012**, *5*, 2013–2024. [CrossRef]
17. Olmo, F.J.; Cazorla, A.; Alados-Arboledas, L.; López-Álvarez, M.A.; Hernández-Andrés, J.; Romero, J. Retrieval of the optical depth using an all-sky CCD camera. *Appl. Opt.* **2008**, *47*, H182–H189. [CrossRef] [PubMed]
18. Kazantzidis, A.; Tzoumanikas, P.; Nikitidou, E.; Salamalikis, V.; Wilbert, S.; Prahl, C. Application of simple all-sky imagers for the estimation of aerosol optical depth. *AIP Conf. Proc.* **2017**, *1850*, 140012. [CrossRef]
19. Román, R.; Antuña-Sánchez, J.C.; Cachorro, V.E.; Toledano, C.; Torres, B.; Mateos, D.; Fuertes, D.; López, C.; González, R.; Lapionok, T.; et al. Retrieval of aerosol properties using relative radiance measurements from an all-sky camera. *Atmos. Meas. Tech.* **2022**, *15*, 407–433. [CrossRef]
20. Shields, J.E.; Karr, M.E.; Johnson, R.W.; Burden, A.R. Day/night whole sky imagers for 24-h cloud and sky assessment: History and overview. *Appl. Opt.* **2013**, *52*, 1605–1616. [CrossRef] [PubMed]
21. Li, X.; Lu, Z.; Zhou, Q.; Xu, Z. A Cloud Detection Algorithm with Reduction of Sunlight Interference in Ground-Based Sky Images. *Atmosphere* **2019**, *10*, 640. [CrossRef]
22. Li, Q.; Lu, W.; Yang, J.; Wang, J.Z. Thin Cloud Detection of All-Sky Images Using Markov Random Fields. *IEEE Geosci. Remote Sens. Lett.* **2011**, *9*, 417–421. [CrossRef]

23. Li, Q.; Lu, W.; Yang, J. A Hybrid Thresholding Algorithm for Cloud Detection on Ground-Based Color Images. *J. Atmos. Ocean. Technol.* **2011**, *28*, 1286–1296. [CrossRef]
24. Ghonima, M.S.; Urquhart, B.; Chow, C.W.; Shields, J.E.; Cazorla, A.; Kleissl, J. A method for cloud detection and opacity classification based on ground based sky imagery. *Atmos. Meas. Tech.* **2012**, *5*, 2881–2892. [CrossRef]
25. Dev, S.; Lee, Y.H.; Winkler, S. Color-Based Segmentation of Sky/Cloud Images From Ground-Based Cameras. *IEEE J. Sel. Top. Appl. Earth Obs. Remote. Sens.* **2016**, *10*, 231–242. [CrossRef]
26. Kazantzidis, A.; Tzoumanikas, P.; Bais, A.; Fotopoulos, S.; Economou, G. Cloud detection and classification with the use of whole-sky ground-based images. *Atmos. Res.* **2012**, *113*, 80–88. [CrossRef]
27. Long, C.N.; Sabburg, J.M.; Calbó, J.; Pagès, D. Retrieving Cloud Characteristics from Ground-Based Daytime Color All-Sky Images. *J. Atmos. Ocean. Technol.* **2006**, *23*, 633–652. [CrossRef]
28. Kamadinata, J.O.; Ken, T.L.; Suwa, T. Sky image-based solar irradiance prediction methodologies using artificial neural networks. *Renew. Energy* **2018**, *134*, 837–845. [CrossRef]
29. Jiang, J.; Lv, Q.; Gao, X. The Ultra-Short-Term Forecasting of Global Horizontal Irradiance Based on Total Sky Images. *Remote Sens.* **2020**, *12*, 3671. [CrossRef]
30. Pawar, P.; Cortés, C.; Murray, K.; Kleissl, J. Detecting clear sky images. *Sol. Energy* **2019**, *183*, 50–56. [CrossRef]
31. Schade, N.H.; Macke, A.; Sandmann, H.; Stick, C. Enhanced solar global irradiance during cloudy sky conditions. *Meteorol. Z.* **2007**, *16*, 295–303. [CrossRef]
32. Frisch-Niggemeyer, A.; Weihs, P.; Revesz, M.; Schreier, S.F.; Richter, A. Relating atmospheric aerosol amounts to blue to red ratio and grayscale contrast fluctuations using digitalization of routine webcam photographs taken in the urban environment of Vienna. *Atmos. Environ.* **2022**, *290*, 119345. [CrossRef]
33. Mayer, B.; Kylling, A. Technical note: The libRadtran software package for radiative transfer calculations—Description and examples of use. *Atmos. Chem. Phys.* **2005**, *5*, 1855–1877. [CrossRef]
34. Emde, C.; Buras-Schnell, R.; Kylling, A.; Mayer, B.; Gasteiger, J.; Hamann, U.; Kylling, J.; Richter, B.; Pause, C.; Dowling, T.; et al. The libRadtran software package for radiative transfer calculations (version 2.0.1). *Geosci. Model Dev.* **2016**, *9*, 1647–1672. [CrossRef]
35. Stamnes, K.; Tsay, S.; Istvan, L. DISORT, a general-purpose Fortran program for discrete-ordinate-method radiative transfer in scattering and emitting layered media: Documentation of methodology. *DISORT Rep.* **2000**, *v1.1.*, 112.